

# Accurate two-dimensional imaging of a human body in motion using multiple ultra-wideband Doppler radar systems in a multipath environment

Hiroki YAMAZAKI<sup>†</sup>, Takuya SAKAMOTO<sup>†</sup>, and Toru SATO<sup>†</sup>

<sup>†</sup> Graduate School of Informatics, Kyoto University  
Yoshida-Honmachi, Sakyo-ku, Kyoto 606-8501, Japan

**Abstract** This paper presents a method of imaging a two-dimensional section of a walking person using multiple ultra-wideband Doppler radar systems. By exploiting multipath echoes, we can increase the effective number of radar systems virtually. Although each simple radar system consists of only two receivers, different line-of-sight velocities allow target positions to be separated and located. The data obtained using the multiple radar systems are integrated using DBSCAN clustering and a target tracking algorithm. Through realistic simulations, we demonstrate the remarkable imaging performance of the proposed method in depicting a clear outline of a human target.

**Key words** ultra-wideband, radar imaging, Doppler radar, human body, multipath

## 1. Introduction

The ability to monitor people automatically has a wide range of applications including home health care of senior citizens and safety monitoring of workers in harsh environments [1], [2]. Ultra-wideband (UWB) radar has remarkable potential as a robust and reliable system for monitoring people, because such systems, unlike optical cameras, can work in adverse environments such as dark, dusty and smoky places with high humidity [3]-[6].

We have developed a simple UWB radar imaging system with three transmitters and six receivers that generates a two-dimensional (2D) sectional shape of the target person, using different line-of-sight velocities of body parts such as the head, body, and limbs. This system first separates multiple echoes from different body parts in the frequency domain [7]. This is followed by interferometric processing to estimate the range and direction of the arrival of each echo. To improve the image quality further, the system continues the same measurement and signal processing for a certain period to collect multiple images. These images are then combined to form a high-quality image of the target by compensating for the target motion [8].

In many scenarios, the received signal contains not only echoes from the target but also clutter components. In such cases, the signal also suffers from ghost echoes from the target that propagate along the multiple paths. In this paper, assuming a person walks along a corridor passage between a pair of parallel walls, we exploit the ghost echoes generated by the multipath environment to improve the imaging

capability, while the number of antennas is reduced to two transmitters and four receivers. The performance of the proposed method is demonstrated in simulations.

To form a radar image, we need to compensate for the motion of targets, which requires the estimation of the target velocity vector. Each radar system, however, can only measure a line-of-sight speed. We need to combine line-of-sight speeds measured using multiple receivers to estimate the velocity vector. It is thus crucial to associate echoes received using different receivers, which is not an easy task. The additional virtual antennas resulting from the multipath effect play an important role in this association. In this paper, we propose a clustering-based algorithm to solve simultaneous equations imposed on target velocity vectors, which also enables association of echoes at the same time. The performance of the proposed method is demonstrated by applying it to simulation data, assuming a person walking along a corridor.

## 2. System Model

The simulated scenario is illustrated in Figs. 1 and 2. Figure 1 illustrates a three-dimensional (3D) scenario with a person walking along a corridor with antennas installed on the ceiling. Figure 2 shows the top view of a narrow passage and a walking person (the torso and arms). For simplicity, we consider a 2D problem with three targets, which are horizontal sections of the target person. In an actual scenario, this model corresponds to the use of antennas that are horizontally omni-directional and vertically directive producing a horizontal fan beam. A person walks towards the bottom

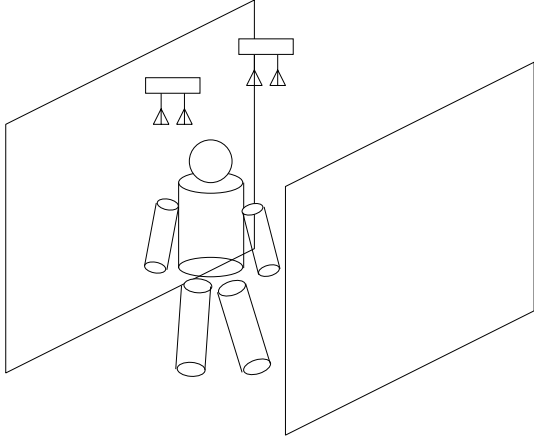


Fig. 1 Assumed scenario with a person walking along a passage.

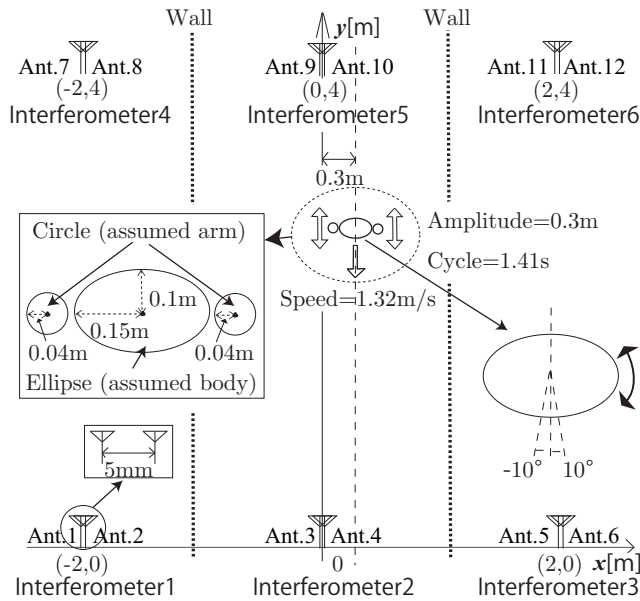


Fig. 2 Schematic of UWB Doppler radar interferometers.

of the figure at an average speed of 1.32 m/s, with both arms swinging in a cycle lasting 1.41 s. The torso and arms are depicted by an ellipse and two circles, respectively. The sizes of the torso and arms are included in the figure.

Using two transmitters and four receivers, we form two groups of one transmitter and two receivers closely located. The two receivers in each group are 5 mm apart, corresponding to half a wavelength. The phase difference between the two receivers is detected to determine the direction of arrival. Thus, each group can be considered an interferometer. We also exploit the mirror images of the actual interferometers (interferometers 2 and 5 in Fig. 2). We use mirror images that include only a single reflection on a wall. Thus, we can use a total of six virtual interferometers as shown in the figure.

In our simulation, received signals are generated using the simple model detailed below. The simulation does not consider waveform distortion, assuming the signal is delayed,

phase-shifted and attenuated depending on the radar cross section of the target and the propagation path length. The transmitted signal has a center angular frequency  $\omega_0 = 2\pi\nu_0$ , and pulse envelope  $T(t)$ , where  $t$  is a fast time. The received echo  $s(t)$  from a single point target after propagating distance  $l$  is then

$$s(t) = \alpha p(t - 2l/c) e^{j(\omega_0 + \omega_d)(t - 2l/c)}, \quad (1)$$

where  $p(t)e^{j\omega_0 t}$  is the transmitted waveform, and  $\omega_d$  is the Doppler angular frequency calculated as  $\omega_d = 4\pi\nu_d\nu_0/c$ , where  $c$  is the speed of light. Considering a typical walking speed of 1.0 m/s, a microwave carrier of 26.4 GHz, and a pulse width of 2.0 ns, we obtain  $\omega_d = 2\pi \times 176$  Hz, which is much smaller than  $\omega_0 = 2\pi \times 26.4$  GHz considering the pulse width of 2 ns. Consequently,  $f_d$  can be reasonably ignored without affecting the results. Note that the Doppler effect exploited in this paper is the phase shift over a pulse-to-pulse interval that is long enough to detect the phase shift.

The received signal from  $N$  targets can be expressed as

$$s(t) = \sum_{n=1}^N \alpha_n p(t - 2l_n/c) e^{j\omega_0(t - 2l_n/c)}, \quad (2)$$

where  $\alpha_n$  is the complex coefficient of the  $n$ -th echo, determined by the radar cross section of the target and propagation path. We simplify the shadowing effect by setting  $\alpha_n = 0$  if the propagation path is blocked by an obstacle. Here,  $\alpha_n$  and  $l_n$  are functions of a slow time  $T$ . In particular, the  $T$ -dependency of  $l_n$  is used to separate multiple targets. The received signal is displayed as  $s(T, t)$ , explicitly showing the dependency on the slow time  $T$ .

### 3. Doppler Interferometry and Imaging

UWB Doppler interferometry [7] separates multiple echoes in the frequency domain and estimates their positions using the phase difference of receivers. If different scattering centers have different radial velocities, they can be separated in a time-frequency analysis employing, for example, a short-time Fourier transform (STFT).

After applying the STFT to data  $s_1(T, t)$  and  $s_2(T, t)$  received by receivers 1 and 2, respectively, we obtain a spectrogram  $S_k(T, \omega)$   $k \in \{1, 2\}$ . Next, we detect the dominant time-frequency points  $(T_i, \omega_i)$  ( $i = 1, \dots$ ) with values greater than the threshold  $|S_k(T, \omega)| > \theta_s$ . From the phase difference  $\Delta\phi_i = \angle S_1(T_i, \omega_i) - \angle S_2(T_i, \omega_i)$ , we can estimate the direction of arrival as

$$\theta = \sin^{-1} \left( \frac{\Delta\phi_i}{2\pi d/\lambda} \right), \quad (3)$$

where  $\lambda$  is the wavelength of the center frequency. Together with the range information, we can estimate the target's position  $\mathbf{x}_i$ .

The above-mentioned method can be applied to each interferometer, leading to multiple sets of image points  $\mathbf{x}_i^m$ , where  $m$  is the interferometer number. Note that each point  $\mathbf{x}_i^m$  is labeled with a radial velocity  $v_i^m$  that can be used to identify image points belonging to the same target, but measured by different interferometers.

Let  $\mathbf{v}$  be the actual velocity of the target, and  $\mathbf{i}_{i_1}^{m_1}$  and  $\mathbf{i}_{i_2}^{m_2}$  be the unit radial vectors between the  $m_j$ -th interferometer and the  $i_j$ -th image point for  $j = 1$  and  $2$ , respectively. The equations

$$\begin{cases} \mathbf{v}^H \mathbf{i}_{i_1}^{m_1} &= v_{i_1}^{m_1}, \\ \mathbf{v}^H \mathbf{i}_{i_2}^{m_2} &= v_{i_2}^{m_2}, \end{cases} \quad (4)$$

then hold, where  $\cdot^H$  is the transpose operator. These simultaneous equations have a solution except when  $\mathbf{i}_{i_1}^{m_1}$  and  $\mathbf{i}_{i_2}^{m_2}$  are parallel. Therefore, if the wrong pair of points is chosen, the resultant velocity  $\mathbf{v}$  is incorrect.

To avoid incorrect estimation of the target velocity, we can add one more condition, by using three interferometers in total to ensure the simultaneous equations have a solution [12]. We thus have

$$\begin{cases} \mathbf{v}^H \mathbf{i}_{i_1}^{m_1} &= v_{i_1}^{m_1}, \\ \mathbf{v}^H \mathbf{i}_{i_2}^{m_2} &= v_{i_2}^{m_2}, \\ \mathbf{v}^H \mathbf{i}_{i_3}^{m_3} &= v_{i_3}^{m_3}. \end{cases} \quad (5)$$

This process suggests that redundancy of the number of antennas is indispensable to avoid erroneous association of echoes from different targets. We assume there are numerous virtual antennas by exploiting the multipath effect, which leads to more stable estimation of the associated echo pairs using the same principle. This idea is discussed in detail in the following section.

#### 4. Proposed Association Algorithm of Echoes using the Doppler Velocity

In our system model, we can use up to six (virtual) antennas as shown in Fig. 2. This allows us to obtain a stable solution for the antenna association problem stated in the previous section. We propose a new method using a clustering algorithm in the velocity space to obtain the most likely combination of echoes that satisfy multiple simultaneous equations such as Eq. (5).

Let us assume that each of the six interferometers detect  $K$  echoes from the received signal. We then need to find likely combinations of echoes out of the  ${}_6C_2 K^2$  combinations. The proposed method proceeds as follows. First, we calculate the simultaneous equations (Eq. (4)) for all the  ${}_6C_2 K^2$  combinations to obtain multiple Doppler velocities. These estimated velocities are displayed on a 2D velocity space  $(v_x, v_y)$ . We then find clusters of data points that have high density, while

leaving other points that are scattered less densely. In this way, we obtain multiple simultaneous equations that have the same solution that corresponds to the actual target velocity.

The  $k$ -means method, a well-known clustering algorithm, is not suited to this purpose because it assigns all the data points to one of the resultant clusters. However, our problem can be solved by finding a few dense clusters while rejecting many more false images generated by wrongly associating inconsistent echoes.

Considering this unique aspect of our problem, we adopt density-based spatial clustering of applications with noise (DBSCAN) [9]. DBSCAN not only separates given data points into multiple clusters but also rejects points that do not form any dense clusters. The actual procedure of DBSCAN is as follows. First,  $\mathbf{p}$ , one of the data points, is randomly selected. Next,  $N(\mathbf{p})$ , which is a set of points within  $D$ -proximity of  $\mathbf{p}$ , is calculated. Then, if  $\mathbf{q}$  satisfies  $\mathbf{q} \in N(\mathbf{p})$  and  $|N(\mathbf{p})| \geq N_{\min}$ ,  $\mathbf{q}$  is classified as a density-reachable point and included in the same cluster as  $\mathbf{p}$ . These steps are iteratively repeated until all the density-reachable points are included in the cluster.

Figure 3 is a schematic showing how DBSCAN works. In the figure, the point  $\mathbf{p}$  is an element of a cluster, and we check if the other points  $\mathbf{p}'$ ,  $\mathbf{q}$ , and  $\mathbf{r}$  belong to the same cluster. The point  $\mathbf{p}'$  is in the same cluster because it is within the  $D$ -proximity of  $\mathbf{p}$ . The point  $\mathbf{q}$  is an element of the same cluster because it is density-reachable from  $\mathbf{p}$  via another point  $\mathbf{p}'$ . In contrast,  $\mathbf{r}$  does not belong to the same cluster because it is not density-reachable from any element of the cluster. In the figure, the  $D$ -proximity of  $\mathbf{q}$  is shown in the image at the bottom. As a result, the point  $\mathbf{r}$  is classified as a false image generated by a wrongly associated echo pair.

The DBSCAN algorithm is first run in 2D velocity space  $v_x$ - $v_y$  and secondary clustering is then performed in 3D time-velocity space  $t$ - $v_x$ - $v_y$ . The former 2D clustering corresponds to solving the simultaneous equations at each time step independently of other time steps. The latter 3D clustering uses the continuity of the target velocity over a short period of time, which is based on the assumption that a human body does not change speed abruptly. Note that the 2D clustering can reduce the number of data points dramatically, and we can thus accelerate the more time-consuming 3D clustering using only a small number of data points. We detect a median point among the points in each resultant cluster. These points are given to the next step for tracking, which is detailed in the next section.

#### 5. Tracking of Clustered Velocities

The clustering procedures are followed by implementation

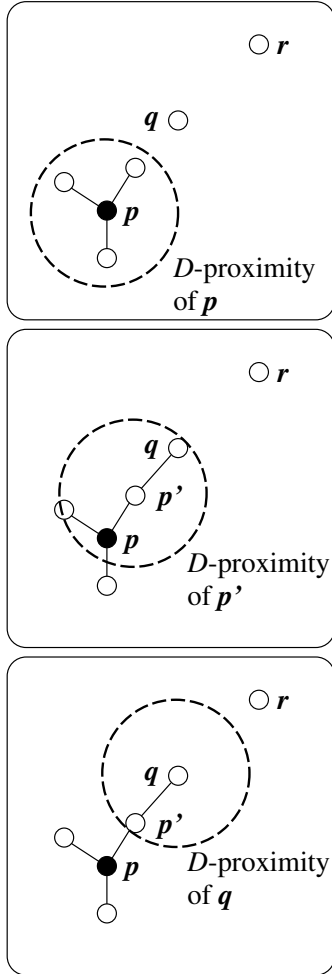


Fig. 3 Schematic of the DBSCAN algorithm.

of a tracking algorithm using an  $\alpha$ - $\beta$  filter [10], [11] to associate the data points over time. Let  $\mathbf{v}(t)$  be one of the estimated target velocities at time  $t$  in the previous section. The  $\alpha$ - $\beta$  filter gives the smoothed velocity  $\mathbf{v}_s(t)$  as

$$\begin{aligned}
 \mathbf{v}_s(t) &= \mathbf{v}_p(t) + \alpha(\mathbf{v}(t) - \mathbf{v}_p(t)), \\
 \mathbf{a}_s(t) &= \mathbf{a}_p(t) + \beta(\mathbf{v}(t) - \mathbf{v}_p(t))/\Delta t, \\
 \mathbf{v}_p(t) &= \mathbf{v}_s(t-1) + \Delta t \mathbf{a}_s(t-1), \\
 \mathbf{a}_p(t) &= \mathbf{a}_s(t-1),
 \end{aligned} \tag{6}$$

where  $\mathbf{v}_p(t)$  is the predicted velocity,  $\mathbf{a}_p(t)$  and  $\mathbf{a}_s(t)$  are the predicted and smoothed accelerations, respectively.

The selection of the points for tracking is determined as

$$|\mathbf{v}(t) - \mathbf{v}_p(t)| \leq D_v, \tag{7}$$

where  $D_v$  is a threshold value. If there are multiple points satisfying this condition, the nearest one is chosen. If there are no points satisfying this condition,  $\mathbf{v}(t) = \mathbf{v}_p(t)$  is assumed.

After the tracking process, we compensate for the motion of each target to form an image corresponding to the initial position  $t = 0.4$  s. Finally, we apply the artifact suppression algorithm [12] to remove artifacts from the image.

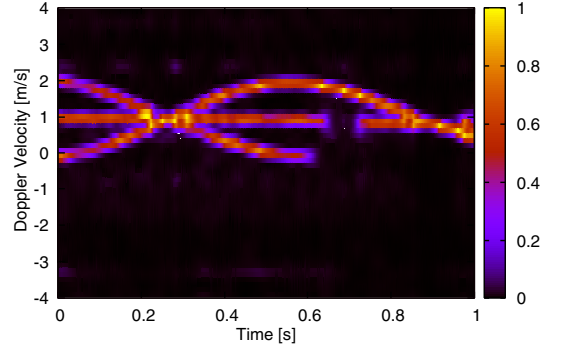


Fig. 4 Spectrogram of a received signal.

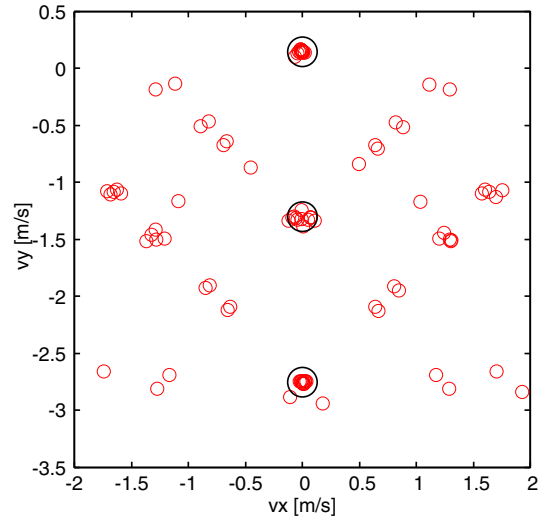


Fig. 5 Target velocities estimated from all possible combinations of interferometers. The actual target velocities are shown as black circles.

## 6. Performance Evaluation of the Proposed Method

We set the parameters for the DBSCAN algorithm as  $D = 0.1$  m/s,  $N_{\min} = 5$ ,  $D_a = 0.2$  m/s,  $D_b = 0.04$  s, and  $N'_{\min} = 30$ , where  $D_a$  and  $D_b$  are the major and minor axes of an ellipsoid defining the proximity in the 3D  $t$ - $v_x$ - $v_y$  space.

Figure 4 shows a simulated spectrogram for one of the signals received using the assumed radar system. We see three trajectories corresponding to the torso and two arms. We detect large peaks from this image to estimate the line-of-sight speeds of the targets. We process the data for  $0.4s \leq t \leq 0.8s$ .

Figure 5 shows the target velocities estimated by solving the simultaneous equation Eq. (4). We see there are numerous candidate points. In the figure, black circles are actual target velocities corresponding to the torso and arms.

After applying the DBSCAN algorithm in the 2D  $v_x$ - $v_y$  space, we obtain the reduced data points shown in Fig. 6. Employing 2D DBSCAN, many of the data points are classi-

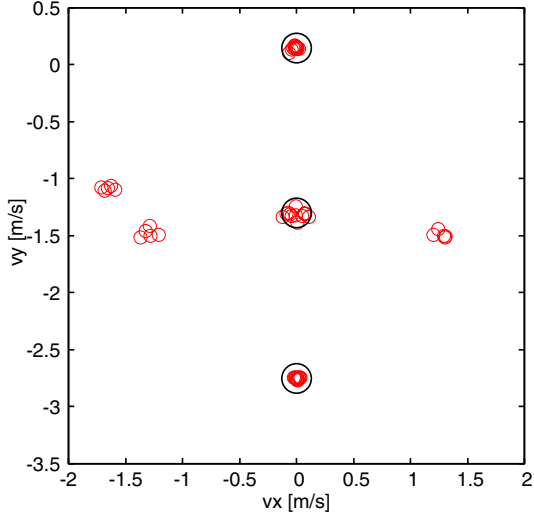


Fig. 6 Output of 2D DBSCAN clustering. Many of the false images are eliminated. The actual target velocities are shown as black circles.

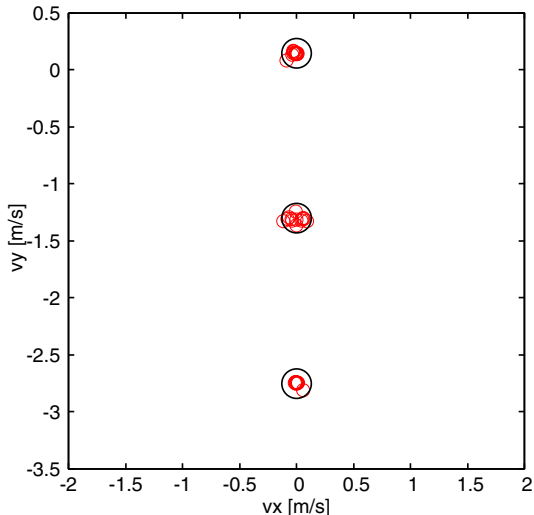


Fig. 7 Output of 3D DBSCAN clustering. Data points are estimated correctly. The actual target velocities are shown as black circles.

fied as artifacts. However, there are still unnecessary points included in the figure.

Finally, we apply 3D DBSCAN in  $t-v_x-v_y$  space, exploiting the time continuity of the actual motion. The resultant data points are shown in Fig. 7. This example demonstrates that the proposed method can accurately estimate target velocities using the clustering approach.

We now know the target velocities, and can thus compensate for the motion to back-propagate the estimated images to the initial position  $t = 0.4$  s to form an image. Figures 8 and 9 are respectively the target image estimated using the proposed method without/with the 3D DBSCAN algorithm or/and artifact suppression. These results show the importance of the information about the time continuity of

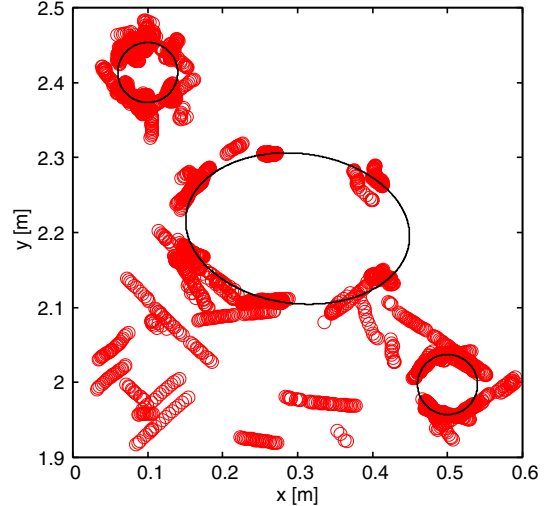


Fig. 8 Target image estimated without 3D clustering or artifact suppression.

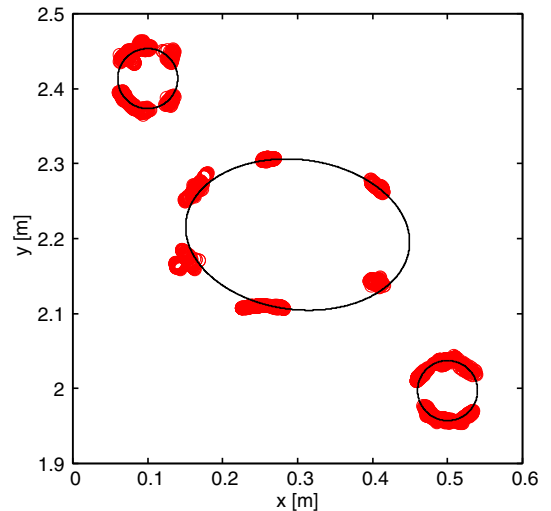


Fig. 9 Target image estimated using the proposed method.

the actual target motion. The image shown in Fig. 9 clearly demonstrates the effectiveness of the proposed method.

## 7. Conclusion

We proposed a new UWB radar imaging algorithm using a couple of Doppler interferometers in a multi-path environment. The multipath effect gives us redundant virtual interferometers, which allows detection of the most probable combination of echoes. We adopted a DBSCAN clustering algorithm to find densely clustered data points, leading to successful estimation of the target motion. The estimated target motion was compensated for to obtain the target image. The result indicates the effectiveness of the proposed method in imaging a realistic target model, simulating a walking person. An important future task is to apply the proposed method to measurement data for an actual human body to demonstrate the performance of the method.

**Acknowledgment** We thank Dr. Kenshi Saho (Ritsumeikan University, Japan) for his help and advice.

### Reference

- [1] S. Nobuhara, Y. Tsuda, T. Matsuyama, and I. Ohama, "Multi-viewpoint silhouette extraction with 3D context-aware error detection, correction, and shadow suppression," *IPSN Trans. Comp. Vis.*, vol. 1, pp. 242–259, 2009.
- [2] A. Mittal and L. S. Davis, "A general method for sensor planning in multi-sensor systems: extension to random occlusion," *Int. J. Comp. Vis.*, vol. 76, no. 1, pp. 31–52, 2008.
- [3] S. Kidera, T. Sakamoto, and T. Sato, "High-resolution and real-time three-dimensional imaging algorithm with envelopes of spheres for UWB radars," *IEEE Trans. Geosci. Remote Sens.*, vol. 46, no. 11, pp. 3503–3513, 2008.
- [4] T. C. Williams, J. M. Sill, and E. C. Fear, "Breast surface estimation for radar-based breast imaging system," *IEEE Trans. Biomed. Eng.*, vol. 44, no. 6, pp. 1678–1686, 2008.
- [5] X. Zhuge and A. G. Yarovoy, "A sparse aperture MIMO-SAR-based UWB imaging system for concealed weapon detection," *IEEE Trans. Geosci. Remote Sens.*, vol. 49, no. 1, pp. 509–517, 2011.
- [6] S. Bertl, A. Dallinger, and J. Detlefsen, "Interferometric focusing for the imaging of humans," *IET Radar Sonar Navig.*, vol. 4, no. 3, pp. 457–463, 2010.
- [7] K. Saho, T. Sakamoto, T. Sato, K. Inoue, and T. Fukuda, "Pedestrian imaging using UWB Doppler radar interferometry," *IEICE Trans. Commun.*, vol. E96–B, no. 2, pp. 613–623, 2013.
- [8] T. Sakamoto, Y. Matsuki, T. Sato, "Method for the three-dimensional imaging of a moving target using an ultra-wideband radar with a small number of antennas," *IEICE Trans. Commun.*, vol. E95–B, no. 3, pp. 972–979, 2012.
- [9] M. Ester, H.-P. Kriegel, J. Sander, and X. Xu, "A density-based algorithm for discovering clusters in large spatial databases with noise," *Proc. 2nd International Conference on Knowledge Discovery and Data Mining*, 1996.
- [10] Y. Kosuge, M. Ito, T. Okada, and S. Mano, "Steady-state errors of an  $\alpha$ - $\beta$ - $\gamma$  filter for radar tracking," *Inc. Electron Comm. Jpn.*, vol. 85, no. 12, pp. 65–79, 2002.
- [11] Y. Kosuge, and M. Ito, "A necessary and sufficient condition for the stability of an  $\alpha$ - $\beta$ - $\gamma$  filter," *Proc. 40th SICE Annual Conference, International Session Papers*, pp. 52–57, 2001.
- [12] H. Yamazaki, K. Saho and T. Sato, "Accurate shape estimation method for multiple moving targets with UWB Doppler radar interferometers," *Proc. International Conference on Space, Aeronautical and Navigational Electronics 2013*, Dec. 2013.